

Numeric Solutions of Eigenvalue Problems for Generic Nonlinear Operators

Ester Hait-Fraenkel¹ and Guy Gilboa

Faculty of Electrical Engineering, Technion, Israel Institute of Technology

Abstract

Numerical methods for solving linear eigenvalue problem are widely studied and used in science and engineering. In this paper, we propose a generalized numerical method for solving eigenproblems for generic, nonlinear operators. This has potentially wide implications, since most image processing algorithms (e.g. denoising) can be viewed as nonlinear operators, whose eigenproblem analysis provides information on the most- and least-suitable functions as input. We solve the problem by a nonlinear adaptation of the power method, a well known linear eigensolver. An analysis and validation framework is proposed, as well as preliminary theory. We validate the method using total-variation (TV) and demonstrate it on the EPLL denoiser (Zoran-Weiss). Finally, we suggest an encryption-decryption application.

Keywords: eigenfunctions, nonlinear operators, denoising, power iteration, total-variation, EPLL

¹Corresponding author, e-mail: etyhait@campus.technion.ac.il

1. Introduction

Linear eigenvalue problems are a fundamental tool for theoretical analysis and deeper understanding of linear operators, as well as for various engineering and scientific applications. Thus, extensive studies were dedicated to finding numerical solutions for the linear eigenvalue problem, $Lu = \lambda u$, where L is a square matrix of size $n \times n$, $u \in \mathbb{C}^{n \times 1}$ is an eigenvector and $\lambda \in \mathbb{C}$ is an eigenvalue. In the rest of the paper we will restrict ourselves to the real setting, and will also often refer to eigenvectors as eigenfunctions. Well-known methods for solving eigenvalue problems are the linear power iteration or power method [1] and the related inverse power method [2].

Recent interest in nonlinear operators and their image processing applications has led to growing research of the generalized *nonlinear* eigenproblem

$$T(u) = \lambda u, \tag{1}$$

where $T(u) : \mathbb{R}^{n \times 1} \rightarrow \mathbb{R}^{n \times 1}$ is a bounded non-linear operator in finite dimensions. So far, methods assumed $T(u)$ is induced by a convex, one-homogeneous functional $J(u)$, such that $T(u)$ is in the subgradient of $J(u)$: $T(u) \in \partial J(u)$. Hein and Buhler [3] extended the inverse power method for non-linear homogeneous functionals (ratio of convex functionals), formulating the iterative scheme as an optimization problem. Nossek and Gilboa [4] suggested an eigenfunction-generating forward flow for operators $p(u)$, where $p(u) \in \partial J(u)$, with $J(u)$ being a convex, one-homogeneous functional. The evolving signal was smoothed in a series of convex minimization steps. Further theoretical analysis and general algorithms are shown in [5],[6],[7],[8].

Recently such algorithms are successfully used in semi-supervised learning, combining deep-nets and graph-based label extension [9].

However, to the best of our knowledge, until now there has been no attempt to solve and analyze eigenproblems for **generic, non-linear** operators. Such operators are very common in signal and image processing, since any nonlinear algorithm (e.g. denoising or deblurring), with same-sized input and output, can be seen as a nonlinear operator, with a discrete input $u \in \mathbb{R}^n$. Lacking any closed-form mathematical formulation, such operators are very complex to characterize, and can be treated as "black-box" operators.

In this paper, we suggest a generalized numerical method to solve and analyze eigenproblems for generic non-linear operators. We show similar interpretations of linear concepts in the adapted nonlinear setting (e.g., large eigenfunctions of denoisers, corresponding to large, highly stable structures, are equivalent to low frequency components for linear smoothing operators). We adapt the well known power iteration to generate eigenfunctions for these "black-box" operators. We establish theoretical requirements for convergence and show steady state properties of our framework. We also provide analysis tools for validation. We showcase our results using the generic non-linear EPLL denoiser [10]. The TV denoising [11] is used for verification, being a well-studied, theoretically-established, functional-based method. Finally, we suggest an application of a decryption-encryption scheme.

The rest of the paper is organized as follows. Sec. 2 presents the method and a theoretical analysis of its properties and behavior. It also shows validation measures, useful induced operators and a method to generate a series of eigenfunctions. Sec. 3 shows experimental results for different operators,

and suggests an application of our method. Sec. 4 concludes our work.

2. Theory and Analysis

In this section, we present the theory and analysis of the generalized power iteration algorithm as adapted for **generic, nonlinear** operators. We denote the evolving signal as $u^k \in \mathbb{R}^{n \times 1}$, and the generic, nonlinear operator used as $T(u) : \mathbb{R}^{n \times 1} \rightarrow \mathbb{R}^{n \times 1}$. $\|\cdot\|$ denotes the ℓ^2 -norm.

2.1. The Linear Case

We shortly display well-known basic concepts of the linear eigenproblem $Lu = \lambda u$, where $\lambda \in \mathbb{R}$ and $u \in \mathbb{R}^{n \times 1}$ are the eigenvalue and eigenfunction, respectively, of the linear operator $L \in \mathbb{R}^{n \times n}$. These concepts will be generalized and extended in our work for generic non-linear problems.

An elementary, widely used numerical method to solve this problem is the *linear power iteration* [1]. In this method, an initial guess f is gradually evolved into the eigenfunction corresponding to a large eigenvalue, by iteratively applying the operator and normalizing the result:

$$u^{k+1} = \frac{Lu^k}{\|Lu^k\|}, \quad (2)$$

initialized with $u^0 = f$, $k = 1, 2, \dots$. For linear operators, its convergence to an eigenfunction can be easily shown (e.g. [12]), with a convergence rate depending on the ratio between the two largest eigenvalues.

Power iteration extensions allow finding additional eigenfunctions. First, to generate a small eigenvalue, power iterations of (2) with an alternative operator, $L^\dagger \equiv I - \alpha L$, [13] yield its large eigenvector, which is a small

one for L (also see [2]). Second, deflation or projection methods (e.g. [14]) generate *more* eigenpairs, relying on previously found eigenvectors of larger eigenvalues. In projection methods, the signal is iteratively projected to the space orthogonal to the known eigenvectors. The Arnoldi iteration [15] uses the Gram-Schmidt process to extract an orthonormal basis, approximating the eigenvectors corresponding to a few large eigenvalues.

Finally, the well-known Rayleigh quotient [16] is defined for real symmetric matrices as:

$$R_{lin}(u) := \frac{u^T L u}{u^T u} = \frac{\langle u, L u \rangle}{\|u\|^2}. \quad (3)$$

Its Euler-Lagrange equation yields the eigenvalue problem, thus any eigenvector is a critical point of the Rayleigh quotient. Moreover, the Rayleigh quotient can be understood as a generalized or approximated eigenvalue computed for any u (not just eigenvectors). For eigenvectors, the Rayleigh quotient is exactly the corresponding eigenvalue λ . These methods and measures will be later generalized into the nonlinear setting.

2.2. Method: Nonlinear Generic Power Iteration

We adapt the *linear* power iteration to generate eigenfunctions for *nonlinear, generic* operators. An initial signal (in our case, image) f evolves using the power iteration method to generate the process $\{u^k\}$:

Algorithm 1. *Power iterations with a generic operator $T(\cdot)$.*

1. *Initialization:* $u^0 \leftarrow f/\|f\|$, $k \leftarrow 1$.
2. *Repeat until $k = K$ or $\|u^{k+1} - u^k\| < \varepsilon$:*
 $u^{k+1} \leftarrow \text{sign}(\langle u^k, T(u^k) \rangle) \frac{T(u^k)}{\|T(u^k)\|}$, $k \leftarrow k + 1$.

For power iterations to be well defined, we assume that $\forall k, 0 < \|T(u^k)\| < \infty$, $T(u^k) \neq 0$, $\langle u^k, T(u^k) \rangle \neq 0$. The result depends on several factors: the initial condition f , the number of iterations, and the operator $T(u)$ and its different parameters (e.g. patch distribution model, estimated noise or estimated blur kernel). We demonstrate these factors (Sec. 3) and even exploit them for our decryption-encryption application. Though our analysis addresses Algorithm 1, in practice we use a slightly modified version. First, we prevent evolution to a trivial constant eigenfunction ($\lambda = \lambda_{max} = 1$ for denoisers) by removing the mean value, such that the signal is of zero mean but of constant variance, preventing a loss of contrast. Second, to handle operators with a desired value range, we modify the normalization stage.

Algorithm 2. *Power iterations for non-trivial solutions.*

1. *Initialization:* $f^0 \leftarrow f^0 - \overline{f^0}$, $k \leftarrow 1$.
2. *Repeat until $k = K$ or $\|u^{k+1} - u^k\| < \varepsilon$:*

$$u^{k+1} \leftarrow T(u^k)$$

$$u^{k+1} \leftarrow u^{k+1} - \overline{u^{k+1}}$$

$$u^{k+1} \leftarrow \frac{u^{k+1}}{\|u^{k+1}\|} \|f^0\|, \quad k \leftarrow k + 1.$$

2.3. Steady State Properties

We analyze the steady state behavior of the process $\{u^k\}$: the relation between convergence and reaching an eigenfunction, and eigenvalue characteristics. Note that at this point, we make minimal assumptions regarding the nature of $T(u)$. Thus, our observations can be applied to any generic, "black-box" operator. General mild assumptions, valid for any reasonable image-processing algorithm, are the existence and non-triviality of $T(u) \forall u$

(e.g. mapping any function to a constant). The existence of eigenfunctions is a broad topic and cannot be proved for any general operator. However, as we show here, convergence immediately implies existence.

Lemma 1. $\forall k, \|u^k\| = 1$.

Proof. Trivial, as each iteration is normalized by the norm: $\|u^k\|^2 = \langle u^k, u^k \rangle = \langle \text{sign}(\langle u^{k-1}, T(u^{k-1}) \rangle) \frac{T(u^{k-1})}{\|T(u^{k-1})\|}, \text{sign}(\langle u^{k-1}, T(u^{k-1}) \rangle) \frac{T(u^{k-1})}{\|T(u^{k-1})\|} \rangle = 1$. \square

Proposition 1. *Algorithm 1 converges after a finite number of steps: $\exists N$ s.t. $\forall k > N, u^{k+1} = u^k$, **if and only if** u^k solves the eigenproblem (1).*

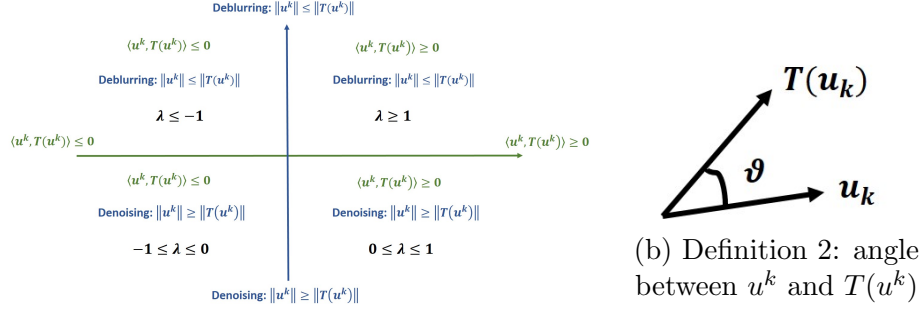
Proof. First, if $\exists N$ such that $\forall k > N, u^{k+1} = u^k$, then $u^k = u^{k+1} = \text{sign}(\langle u^k, T(u^k) \rangle) \frac{T(u^k)}{\|T(u^k)\|}$. Thus, $T(u^k) = \text{sign}(\langle u^k, T(u^k) \rangle) \|T(u^k)\| u^k = \lambda u^k$, where $\lambda = \text{sign}(\langle u^k, T(u^k) \rangle) \|T(u^k)\|$.

Second, if some iterate u^k admits (1), then by taking the inner product with u^k on both sides we reach $\text{sign}(\langle u^k, T(u^k) \rangle) = \text{sign}(\lambda)$. Using the definition of u^{k+1} and Lemma 1 we get $u^{k+1} = \text{sign}(\langle u^k, T(u^k) \rangle) \frac{T(u^k)}{\|T(u^k)\|} = \text{sign}(\lambda) \frac{\lambda u^k}{\|\lambda u^k\|} = u^k$. Thus, the process converges. \square

Several reasonable assumptions can be made regarding the nature of T :

1. If T is a denoising (coarsening) operator, then $\forall k, \|u^k\| \geq \|T(u^k)\|$.
2. If T is a deblurring (sharpening) operator, then $\forall k, \|u^k\| \leq \|T(u^k)\|$.
3. $\forall k, \langle u^k, T(u^k) \rangle \geq 0$. Positive correlation between input and processed input (typical in denoising).
4. $\forall k, \langle u^k, T(u^k) \rangle \leq 0$. Negative correlation (rare).

Corollary 1. *Eigenvalue range. If u^k is a converged solution of Algorithm 1, that is, $T(u^k) = \lambda u^k$, then the following holds w.r.t. the eigenvalue λ :*



(a) Corollary 1: eigenvalue sign and magnitude

Figure 1: Illustrations of Corollary 1, Definition 2.

1. $\lambda = \text{sign}(\langle u^k, T(u^k) \rangle) \|T(u^k)\|$.
2. If assumptions 1, 3 hold, then $0 \leq \lambda \leq 1$. If assumptions 1, 4 hold, then $-1 \leq \lambda \leq 0$. That is, for a denoising operator, $|\lambda| \leq 1$.
3. If assumptions 2, 3 hold, then $\lambda \geq 1$. If assumptions 2, 4 hold, then $\lambda \leq -1$. That is, for a deblurring operator, $|\lambda| \geq 1$.

The above can be easily verified using the proof of Proposition 1, Lemma 1 and the respective assumptions. For example, to show the first assertion of point (2) above: Assumption 1 and Lemma 1 yield $1 = \|u\| \geq \|T(u)\| = |\lambda|$, whereas from point (1) above, proved in the proposition, and Assumption 3 we have: $\text{sign}(\lambda) = \text{sign}(\langle u^k, T(u^k) \rangle) \geq 0$, thus we conclude $0 \leq \lambda \leq 1$.

2.4. Eigenfunction Validation Measures

The numerical method suggested here for eigenfunction computation, with no analytic solutions, obliges us to verify our results. Thus, we propose several easy to calculate validation measures, in order to verify the convergence of our method to eigenfunctions (up to some minor error). We discuss their behavior throughout the power iteration and in steady state, and show

their usefulness for validating that a specific signal is an eigenfunction.

Point-wise validation and visualization. At the risk of stating the obvious, the most fundamental validation measure for an eigenfunction u is that it must admit: $T(u) = \lambda u$, for some constant $\lambda \in \mathbb{R}$. Specifically for images (which are our focus here), this means that each pixel (i, j) must hold $\lambda = T(u)_{ij}/u_{ij}$. Thus, when visualizing the ratio $T(u)/u$, we should ideally obtain a constant image. This visualization can also point out image regions of less accuracy, e.g. near zero values, where the denominator of the measure is less stable. It should also hold for a specific image row/ column. This is obviously also a simple way of finding the corresponding eigenvalue.

Global indicators. First, we generalize the Rayleigh quotient [16] for non-linear operators:

Definition 1. *The Rayleigh quotient of u^k is defined as*

$$R(u^k) = \frac{\langle u^k, T(u^k) \rangle}{\|u^k\|^2}. \quad (4)$$

The measure was also defined and investigated for nonlinear operators induced by a one-homogeneous functional $J(u)$ [4] as follows: $R(u) = \frac{J(u)}{\|u\|^2}$. The definition of (4) generalizes [4], since for one-homogeneous functionals $J(u) = \langle u, p(u) \rangle$, where $p(u)$ is a subgradient element of $J(u)$, and $T(u) = p(u)$. It also naturally generalizes the linear case (3), by setting $T(u) = L(u)$.

Proposition 2. $\forall k, |R(u^k)| \leq \|T(u^k)\|$. *Equality holds **if and only if** u^k is an eigenfunction, admitting (1).*

Proof. Using Lemma 1 and the Cauchy-Schwarz inequality:

$$|R(u^k)| = \left| \frac{\langle u^k, T(u^k) \rangle}{\|u^k\|^2} \right| = |\langle u^k, T(u^k) \rangle| \leq \|u^k\| \|T(u^k)\| = \|T(u^k)\|.$$

The Cauchy-Schwarz then holds in equality if and only if u^k and $T(u^k)$ are linearly dependent, that is, u^k is a solution of the eigenproblem (1). \square

Proposition 3. *Suppose that exactly at iteration $k = N$ Algorithm 1 converged. Then $\forall k < N$, $|R(u^k)| < \|T(u^k)\|$, $\forall k \geq N$, $|R(u^k)| = \|T(u^N)\|$.*

Proof. Follows directly from Propositions 1 and 2. \square

Since the algorithm converges when the Rayleigh quotient stabilizes, its stabilization is a good indication for convergence. Then the value of the Rayleigh quotient is also the eigenvalue. In practice, for the operators tested, the Rayleigh quotient monotonically increases to the eigenvalue (see Sec. 3).

Another global measure is the angle between u^k and $T(u^k)$ (Fig. 1b), inspired by a similar definition in [4] for their subgradient-induced operator.

Definition 2. *The cosine of the angle between u^k and $T(u^k)$ is defined as*

$$\cos\theta = \frac{\langle u^k, T(u^k) \rangle}{\|u^k\| \|T(u^k)\|}. \quad (5)$$

Proposition 4. *The angle between u^k and $T(u^k)$ is πn , $n \in \mathbb{Z}$ **if and only if** u^k solves the eigenproblem (1).*

Proof. First, (1) means that $\cos\theta = \frac{\langle u^k, T(u^k) \rangle}{\|u^k\| \|T(u^k)\|} = \frac{\langle u^k, \lambda u^k \rangle}{\|u^k\| \|\lambda u^k\|} = \pm 1$.

Second, suppose that the angle between u^k and $T(u^k)$ is πn . Then $\pm 1 = \cos\theta = \frac{\langle u^k, T(u^k) \rangle}{\|u^k\| \|T(u^k)\|} \xRightarrow{\text{Lemma 1}} \langle u^k, T(u^k) \rangle = \pm \|T(u^k)\| \implies |\langle u^k, T(u^k) \rangle| = \|T(u^k)\|$. From Proposition 2, this only holds if u^k and $T(u^k)$ are co-linear. Thus, (1) holds with $\lambda = \pm \|T(u^k)\|$. \square

2.5. Contraction Operators

So far we have discussed the steady state behavior of the power iteration for a very generic $T(u)$, making very few assumptions regarding its nature. We will now follow previous work (e.g. [17], [18], [19], [20]) treating the power iteration process as a fixed-point process (note, that applying the fixed-point iteration for functionals has been investigated before [21]). We will also make the reasonable assumption that $T(u)$ is a *contraction operator* (defined hereafter). Under this assumption we prove the *convergence* of this process. In Sec. 3 we test if our nonlinear operators indeed behave as contraction operators. We will show that while the stronger condition does not hold, a weaker but sufficient condition does hold, and thus this assumption is valid.

We write the power iteration process $\{u^k\}$ as the fixed-point process $\{g^k\}$:

Algorithm 3. *Power Iteration as a Fixed-point Process.*

1. *Initialization:* $g^0 \leftarrow f^0$, $\|f^0\| = 1$, $k \leftarrow 1$.
2. *Repeat until* $k = K$ *or* $\|g^{k+1} - g^k\| < \varepsilon$:
 $g(u^k) \equiv u^{k+1} \leftarrow \text{sign}(\langle u^k, T(u^k) \rangle) \frac{T(u^k)}{\|T(u^k)\|}$, $k \leftarrow k + 1$.

Proposition 5. *The fixed-point iteration process $\{g^k\}$ converges, that is, $\lim_{k \rightarrow \infty} \|u^k - u^{k-1}\| = 0$, if g is a contraction operator, that is, if $\forall x, y$, there exists $L < 1$, such that g admits the following Lipschitz continuity property: $\|g(x) - g(y)\| \leq L\|x - y\|$.*

Proof. This follows the Banach fixed point theorem. Following the Lipschitz continuity assumption, $\exists L < 1$ such that the following statements hold:

$$\begin{aligned} \|u^2 - u^1\| &\equiv \|g(u^1) - g(u^0)\| \leq L\|u^1 - u^0\| \\ \|u^3 - u^2\| &\equiv \|g(u^2) - g(u^1)\| \leq L\|u^2 - u^1\| \leq L^2\|u^1 - u^0\| \quad \dots \end{aligned}$$

$$\|u^k - u^{k-1}\| \equiv \|g(u^{k-1}) - g(u^{k-2})\| \leq L\|u^{k-1} - u^{k-2}\| \leq L^{k-1}\|u^1 - u^0\|$$

Now, for $L < 1$, $\lim_{k \rightarrow \infty} \|u^k - u^{k-1}\| \leq \lim_{k \rightarrow \infty} L^{k-1}\|u^1 - u^0\| = 0$, hence $\lim_{k \rightarrow \infty} \|u^k - u^{k-1}\| = 0$. \square

2.6. Induced Operators

We present a useful concept of operators induced by a given **generic, non-linear** operator, which allow generating eigenfunctions with different characteristics than those of the given operator. Most importantly, the complementary operator defined here easily allows generating eigenfunctions corresponding to the *small* eigenvalue of the given operator.

Definition 3. *Complementary operator. The complementary operator corresponding to the generic operator $T(u)$ is defined as: $T^\dagger(u) \equiv u - T(u)$, such that $T + T^\dagger = I$, where I is the identity operator.*

Property 1. *If u is an eigenfunction of $T(u)$ with an eigenvalue λ , then u is also an eigenfunction of $T^\dagger(u)$ with an eigenvalue $(1 - \lambda)$.*

Since $\{u, \lambda\}$ are an eigenpair of $T(u)$ we have $T(u) = \lambda u$. Thus: $T^\dagger(u) \equiv u - T(u) = u - \lambda u = (1 - \lambda)u$. Therefore, $\{u, (1 - \lambda)\}$ are an eigenpair of $T^\dagger(u)$. From Property 1, the following useful property immediately follows:

Property 2. *The eigenfunction corresponding to the large eigenvalue of $T^\dagger(u)$ is the eigenfunction corresponding to the small eigenvalue of $T(u)$.*

A useful algorithmic property thus results. Since Algorithm 1 generates an eigenfunction with the maximal possible eigenvalue (as seen numerically), applying it using T^\dagger will generate an eigenfunction of T with the *minimal* possible eigenvalue. This is a natural extension of the linear case.

Remark 1. For T with $\lambda \in [0, 1]$ (a typical behavior for coarsening (denoising) operators), we get $\lambda \in [0, 1]$ also for T^\dagger .

Remark 2. For $[0, \lambda_{max}]$ with $\lambda_{max} > 1$, we can attain positive eigenvalues for T^\dagger using the following variant: $T^\dagger := I - \alpha T$, where $\alpha \leq \frac{1}{\lambda_{max}}$.

We focus on denoising operators, designed to remove noise or simplify the image by removing fine-scale details, thus refer to T^\dagger as a *texture generator*.

We also define an *enhancing operator* by adding the textural part, weighted by α : $T_\alpha^E(u) \equiv u + \alpha T^\dagger(u) = u(1 + \alpha) - \alpha T(u)$, where $\alpha > 0$.

In this case, if u is an eigenfunction of $T(u)$ with an eigenvalue λ , then u is also an eigenfunction of $T_\alpha^E(u)$, with an eigenvalue $(1 + \alpha - \alpha\lambda) \geq 1$.

2.7. Generating More Eigenfunctions

As mentioned before, Algorithm 1 generates a single eigenfunction (given f^0) with λ very close to 1. Additionally, as discussed following Property 2, applying Algorithm 1 with T^\dagger results in an eigenfunction of T with a small eigenvalue. We now address the problem of obtaining additional eigenfunctions stemming from f^0 , following projections methods in the linear case.

Definition 4. Let $\{v_i\}_{i=1}^N$ be an orthonormal set of eigenfunctions of T , that is, each v_i admits (1) and in addition, $\forall i, j, \langle v_i, v_j \rangle = \delta_{ij}$. Then a **single projection** of f onto the space **orthogonal** to $\{v_i\}_{i=1}^N$ is defined as: $f_N = f - \sum_{i=1}^N \langle f, v_i \rangle v_i$.

The resulting projection f_N is then orthogonal to the set $\{v_i\}_{i=1}^N$:

Property 3. $\forall 1 \leq j \leq N, \langle v_j, f_N \rangle = 0$.

Proof. $\langle v_j, f_N \rangle = \langle v_j, f \rangle - \sum_{i=1}^N \langle f, v_i \rangle \langle v_i, v_j \rangle \stackrel{\text{Orthonormality}}{=} \langle v_j, f \rangle - \sum_{i=1}^N \langle f, v_i \rangle \delta_{ij} \stackrel{\text{Sum is 0 only for } i=j}{=} \langle v_j, f \rangle - \langle f, v_j \rangle = 0. \quad \square$

Now, to attain v_{N+1} , we initialize the process with f^N , a single projection of f^0 . We then iteratively apply T and perform a single projection:

Algorithm 4. *Generating More Eigenfunctions.*

1. *Initialization:* f^N , $k \leftarrow 1$.
2. *Repeat until $k = K$ or $\|u^{k+1} - u^k\| < \varepsilon$:*
 - $z^k \leftarrow T(u^k)$;
 - $y^k \leftarrow \text{single projection of } z^k$;
 - $u^{k+1} \leftarrow \frac{y^k}{\|y^k\|}$, $k \leftarrow k + 1$.

Remark. For a non-orthogonal set of eigenfunctions, projection should be done iteratively: $f_1 = \frac{\langle f, v_1 \rangle v_1}{\|v_1\|^2}$, $f_2 = \frac{\langle f_1, v_2 \rangle v_2}{\|v_2\|^2}$, and so on.

It can be easily seen that when the process reaches an eigenfunction, it converges, assuming orthogonality of previous eigenfunctions, and the result is also orthogonal to previous ones. In practice, the *function* generated is orthogonal to the set, though we cannot guarantee this. However, it may be considered only as a *pseudo*-eigenfunction, as it may not hold $T(u) = \lambda u$. Nevertheless, we can generate an eigenfunction admitting (1) by applying more power iterations without projectios, at the expense of orthogonality. This agrees with recent TV and one-homogeneous functionals [22, 23, 24] theory, where eigenfunctions are not necessarily orthogonal.

3. Experimental Results and Applications

In this section, we present experimental results for generating eigenfunctions of different generic, non-linear operators, both denoisers and, apparently for the first time, non-convex deblurring operators. We first validate

our method using the well-established TV denoiser. We then show results for the "black-box" generic non-linear EPLL denoiser, and suggest an application of a decryption-encryption scheme. For both denoisers, we also show eigenfunction degradation robustness and decay profiles. Last, we demonstrate our method for the TV and EPLL deblurring operators.

We denote the degraded image, the restored image, the eigenvalue and the blurring kernel as f , u , λ and A , respectively. When formulating optimization problems, $\eta > 0$ is a fixed weight between the fidelity and prior terms. x is a pixel in image domain Ω . We empirically determine the number of iterations, such that the result admits the eigenfunction validation measures.

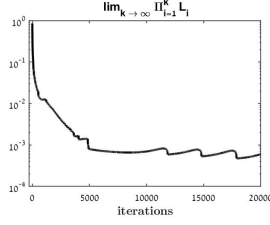
3.1. Validation: TV Denoising Operator

We show results for the well-established non-linear TV denoiser [11], which can be formulated as the following optimization problem:

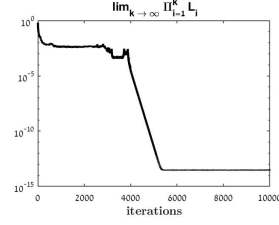
$$\min_u \frac{\eta}{2} \|f - u\|^2 + \int_{\Omega} |\nabla u(x)| dx, \quad (6)$$

This section serves two purposes. Applying our method to a well-studied, mathematically-formulated operator serves as a proof of concept for our method, as we compare our results to known ones. We also present first results on the TV texture generator (eigenfunctions with small eigenvalues).

To apply our method to the TV denoiser, we first test (Fig. 2a) whether TV behaves as a contraction operator. While the stronger Lipschitz condition $L_k < 1$ ($L_k = \frac{\|u^k - u^{k-1}\|}{\|u^{k-1} - u^{k-2}\|}$) does not hold numerically $\forall k$, a weaker but sufficient condition holds: $\lim_{k \rightarrow \infty} \prod_{i=1}^k L_i = 0$. Thus, the process converges, yielding an eigenfunction (Propositions 5, 1).



(a) Weak condition holds for TV



(b) Weak condition holds for EPLL

Figure 2: TV and EPLL hold a weak condition for being contraction operators: $\lim_{k \rightarrow \infty} \prod_{i=1}^k L_i = 0$ ($L_k = \frac{\|u^k - u^{k-1}\|}{\|u^{k-1} - u^{k-2}\|}$), thus the process converges (Proposition 5).

Fig. 3 shows the power iteration evolution of an initial image to the final eigenfunction. Note that the eigenvalue is smaller than but very close to 1, as expected from a detail-attenuating operator, and in accordance with Corollary 1. The eigenfunction represents the coarse structure of the initial image, and its shape is in accordance with the convex nature of TV eigenfunctions [25]. We also validate (Sec. 2.4) that this is an eigenfunction. Note that the specific method of discretization can affect the eigenfunction structure (we use [26]). Fig. 4a-4b shows the eigenfunction decay when the denoiser is iteratively applied: for 98% of pixels, decay profiles exhibit a distinct pattern, consistent with the theory of TV eigenfunctions [23] as analyzed in the context of decay profiles in [27].

Last, we present the induced TV texture generator and generate its eigenfunction (Fig. 5), which is with an eigenvalue of 1. This is also the small eigenfunction of the TV denoiser with eigenvalue 0 (see Property 2). Indeed TV denoising (6) can yield a solution $u = 0$, when TV of u^k is high enough (depending on η) [28] (see a generalization for arbitrary 1-homogeneous functionals in [29]). Indeed the final result represents the texture of the initial image. Again, we validate this is an eigenfunction.

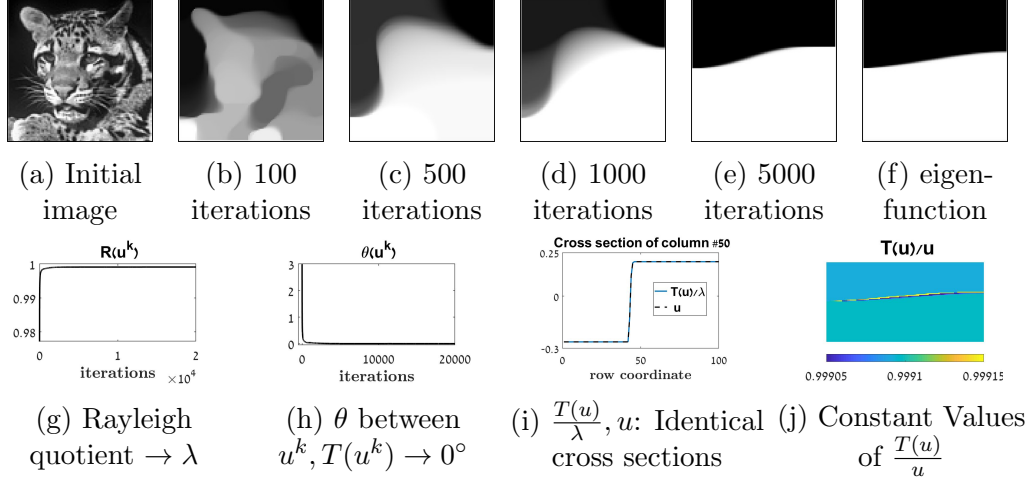


Figure 3: TV power iteration evolution to final eigenfunction u (20,000 iterations) with $\lambda = 0.9991$. We validate this is an eigenfunction: the Rayleigh quotient increases to the eigenvalue (in accordance with Propositions 2, 3), and the angle between $u^k, T(u^k)$ decreases to zero (in accordance with Proposition 4). Cross sections of $\frac{T(u)}{\lambda}, u$ are identical, and $\frac{T(u)}{u} = C$ (98% of values are in the displayed range).

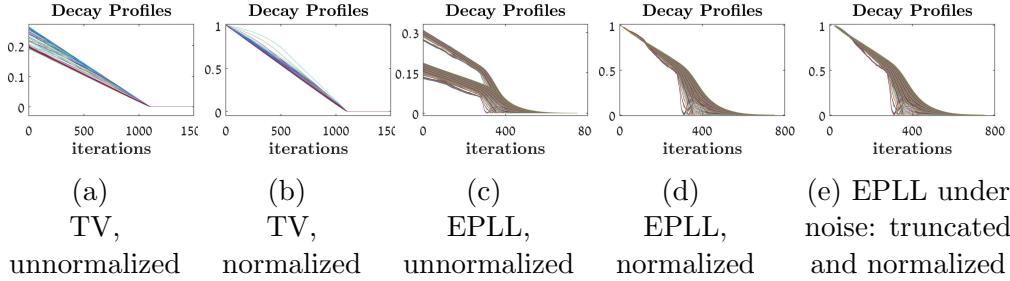


Figure 4: Decay profiles (per pixel) of eigenfunctions, when the corresponding denoiser is iteratively applied. (a)-(b): TV decay profiles show a distinct pattern, consistent with TV theory. (c)-(d): EPLL decay profiles also show a distinct pattern (though there is no EPLL theory for comparison). (e): We truncate the distorted beginning of EPLL decay profiles of a degraded eigenfunction (noise, $\sigma = 0.1$), which results in similar profiles.

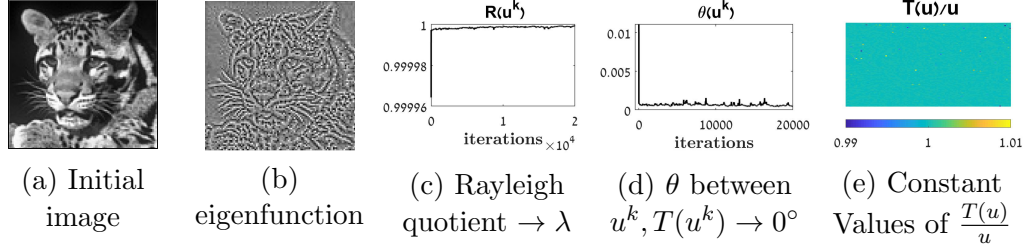


Figure 5: TV texture generator eigenfunction u , with $\lambda = 1$. We validate this is an eigenfunction following Propositions 2-4. Also, $\frac{T(u)}{u} = C$ (99.9% of values are in the displayed range).

3.2. EPLL Denoising Operator

We show experimental results for the "black-box" generic non-linear EPLL (Expected Patch Log Likelihood) denoiser [10]. EPLL uses a generic framework for efficient image restoration, using a prior p on image patches (selected using the operator P_i), formulated as the following optimization problem:

$$\min_u \frac{\eta}{2} \|f - u\|^2 - EPLL_p(u), \quad EPLL_p(u) = \sum_i \log p(P_i u) \quad (7)$$

To increase performance, the paper suggests using the simple Gaussian Mixture Model (GMM) prior, learned from a set of natural images: $\log p(x) = \log \left(\sum_{k=1}^K \pi_k N(x \mid \mu_k, \Sigma_k) \right)$, where K , π_k , μ_k , Σ_k are the number of Gaussian mixtures, their mixing weights, their means and their covariance matrices, respectively. EPLL was shown to prefer large structures, straight borders and round corners [30].

We first apply our method to the EPLL denoiser itself to generate a large eigenfunction. Note that we drop the output clipping stage within EPLL to avoid evolution in the linear region of the operator. We first test (Fig. 2b) whether EPLL behaves as a contraction operator. Again, a weaker but

sufficient Lipschitz condition holds: $\lim_{k \rightarrow \infty} \prod_{i=1}^k L_i = 0$. Thus, the process converges, and converges into an eigenfunction (Propositions 5, 1).

Fig. 6 shows the power iteration evolution of two different initial images to the final eigenfunctions. Note that the eigenvalues are smaller than but very close to 1. This is as expected from a detail-attenuating operator, and is in accordance with Corollary 1. Eigenfunctions are different, as each represents the coarse structure of a different initial image, and their shapes are in accordance with the observations made in [30]. We also validate these are eigenfunctions, where we see a similar behavior for both eigenpairs. Fig. 7 shows a known eigenfunction behavior: using the corresponding denoiser, noise is better removed from the large eigenfunctions, than from natural images, and from small eigenfunctions.

Fig. 4c-4d shows the distinct pattern of decay profiles for 97% of pixels. Obviously, as opposed to TV, EPLL has no decay profile theory to compare to. Following Sec. 2.7, we generate the second large eigenfunction (Fig. 8), orthogonal to the large eigenfunction. However, the process keeps evolving and thus does not hold (1). Thus, it can only be considered as a **pseudo**-eigenfunction (see [4]). Finally, Fig. 9 shows the large eigenfunction of the EPLL texture generator, with an eigenvalue very close to 1. This is also a small eigenfunction of the EPLL denoiser, following Property 2 (it is also easy to validate that Property 1 indeed holds), and indeed, it represents the texture of the initial image. We also validate this is an eigenfunction.

Fig. 10 demonstrates eigenfunction robustness to various small degradations. The Rayleigh quotient of a degraded eigenfunction is similar to that of a "clean" one, and power iterations make it converge to the critical point in

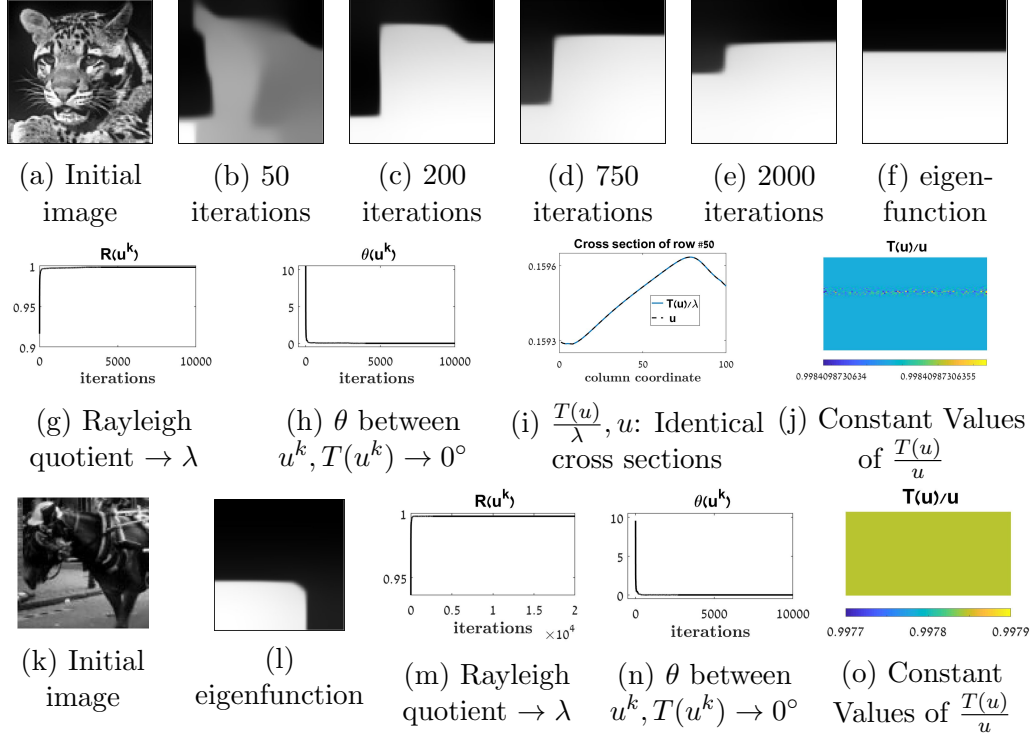


Figure 6: EPLL power iteration evolutions to final eigenfunctions u . Top rows: 10,000 iterations of tiger image, $\lambda = 0.9984$. Bottom row: 20,000 iterations of horse image, $\lambda = 0.9978$. We validate these are eigenfunctions following Propositions 2-4. Also, cross sections of $\frac{T(u)}{\lambda}, u$ are identical, and $\frac{T(u)}{u} = C$ (all values are in the displayed ranges).

the vicinity - the original eigenvalue. Especially note the important property of "small message" robustness that will be used for the decryption-encryption application (Sec. 3.3). Note that noise robustness holds in a very wide sense. For example, the denoiser considers textures and fine details as noise, which can be removed. The texture generator, on the other hand, prefers noise and textures, and thus considers coarse structures as noise. The decay profiles of a degraded eigenfunction also exhibit a distinct pattern (Fig 4e), similar to those of the "clean" eigenfunction, but sometimes distorted in the beginning.

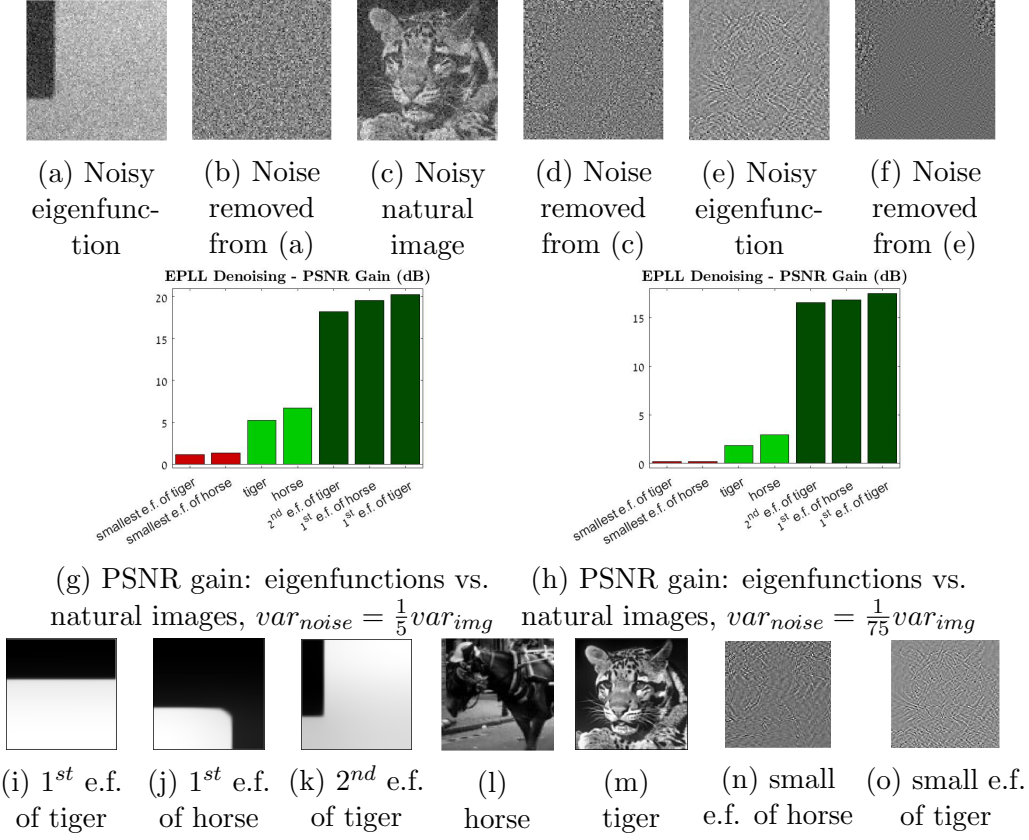


Figure 7: Demonstration (for EPLL) of a known eigenfunction property: a denoiser better denoises its large eigenfunctions, than natural images, than its small eigenfunctions. When noising with $var_{noise} = \frac{1}{5}var_{img}$ and denoising with EPLL, more noise is removed from the 2nd eigenfunction (b), than from a natural image (d), than from the small eigenfunction (f), and it is more uniform. (g-h): PSNR gain when denoising using EPLL for different noise levels and different images (i-o): eigenfunctions vs. natural images.

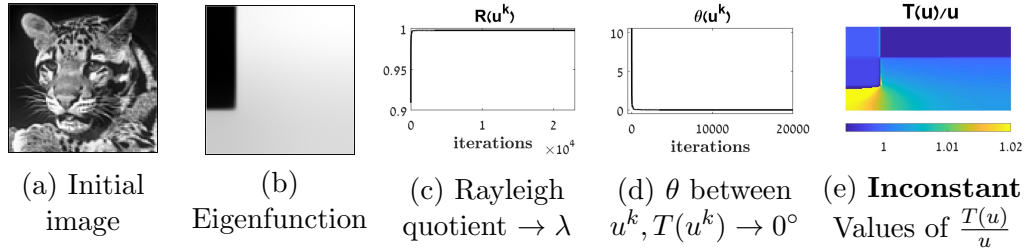


Figure 8: EPLL 2nd large eigenfunction u , with $\lambda = 0.9977$. We validate that Propositions 2-4 hold. However, as $\frac{T(u)}{u} = C$ does not hold, this is only a **pseudo**-eigenfunction.

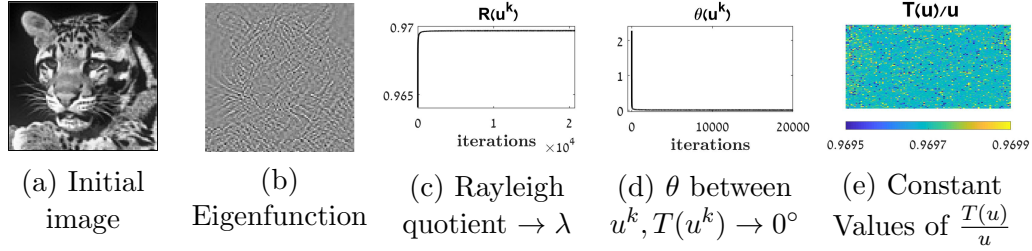


Figure 9: EPLL texture generator eigenfunction u , with $\lambda = 0.9697$. We validate this is an eigenfunction following Propositions 2-4. Also, $\frac{T(u)}{u} = C$ (96% of values are in the displayed range).

3.3. Application: Encryption-Decryption Scheme

We suggest an encryption-decryption scheme and demonstrate it for the EPLL denoiser. We exploit eigenfunction robustness to adding a "small message" (Fig. 10f), which can be removed by applying power iterations. Then, the difference image will reveal the message, which may be too small to be detected in the original image. We also exploit the strong impact of parameters chosen to generate the eigenfunction (Sec. 2.2), which can be decided by the sender and secretly shared with the receiver. However, as they are unknown to enemies, decryption is practically impossible for them.

Fig. 11 shows the three components of the scheme. First, the sender decides on different impacting factors, generates the eigenfunction, and adds the secret hidden message. Second, the receiver uses the secret impacting factors to apply power iterations to remove the message. Some simple post-processing may also be needed. Third, enemies try to decrypt the hidden message using the power iteration with unknown factors. More specifically, the prior model for EPLL, GMM, offers numerous options of covariance matrices, mixing weights and component numbers, which are practically impossible to guess. Thus the enemies fail, and the message remains hidden. Fig.

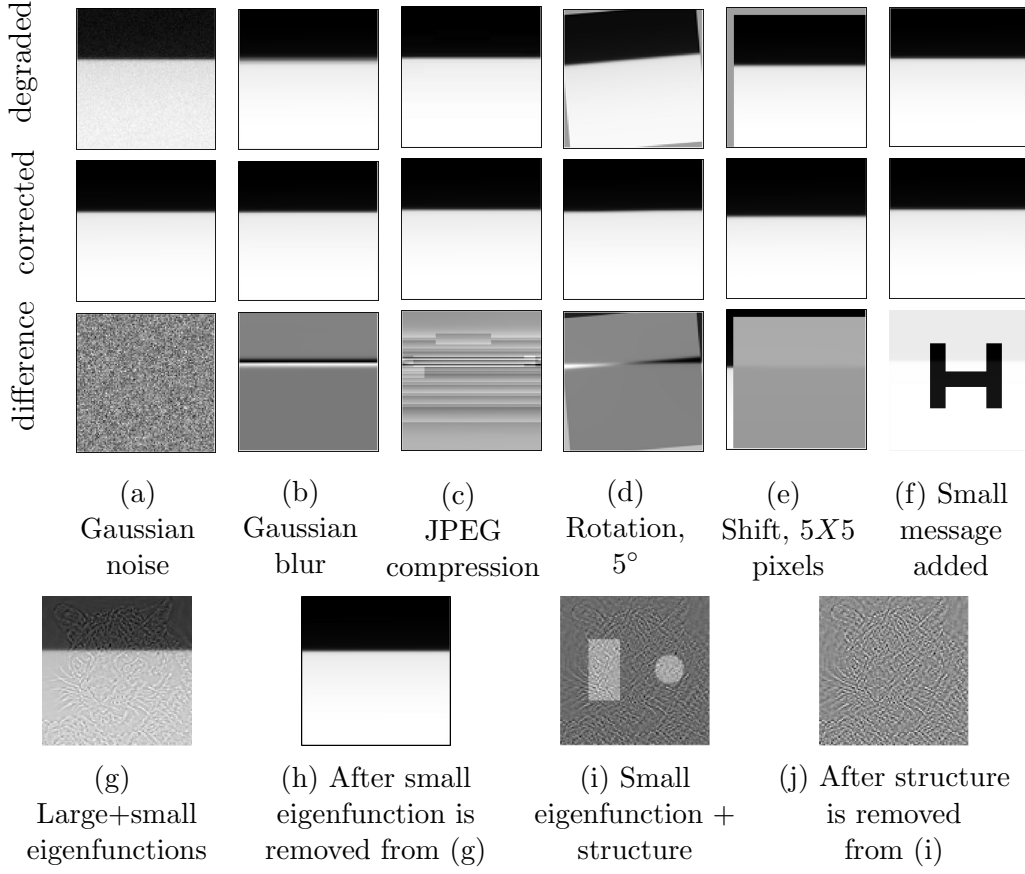


Figure 10: (a)-(f): Degradation robustness of EPLL large eigenfunction for various small degradations. Top: degraded eigenfunctions (e.g. noise of $\sigma = 0.01$, blur of $\sigma = 0.01$, see different columns). Middle: corrected eigenfunctions after applying 500 power iterations. Bottom: Difference images. (g)-(h): A small eigenfunction, added to the large, is considered by the denoiser as "noise", and thus removed. (i)-(j): A structure, added to the small eigenfunction, is considered by the texture generator as "noise", and thus removed.

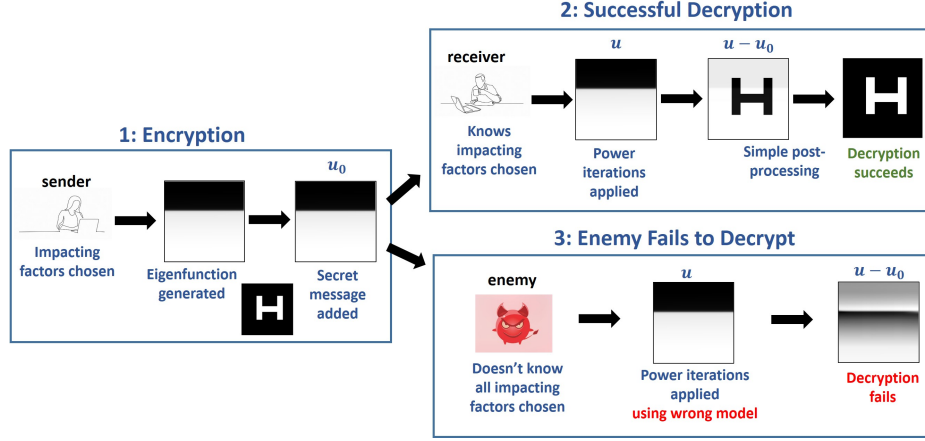


Figure 11: Flow chart: encryption-decryption application. The receiver applies power iterations with secret impacting factors to decrypt the message. However, enemies apply power iterations with unknown factors and thus fail to decrypt.

12 shows several examples of the application.

3.4. Deblurring Operators

To the best of our knowledge, this is the first attempt to find eigenpairs for non-convex deblurring operators (but see [31], [29]). In the absence of previous theory, we use our knowledge of sharpening operators and specific priors and our analysis in Sec. 2 for analysis. The possible meaning in this context of a complementary operator, the small eigenfunction, or an equivalence to decay profiles, remains for now an open question.

Both deblurring operators examined, TV and EPLL, can be formulated as optimization problems similar to Eq. 6, 7, respectively, with an adapted fidelity term: $\|f - Au\|^2$. We also note that we slightly update the power iteration scheme: mean is kept as $\overline{f^0}$ for f^0 and throughout evolution.

Fig. 13 shows results for both operators. We show different large eigenfunctions of the EPLL deblurring operator, generated using different motion

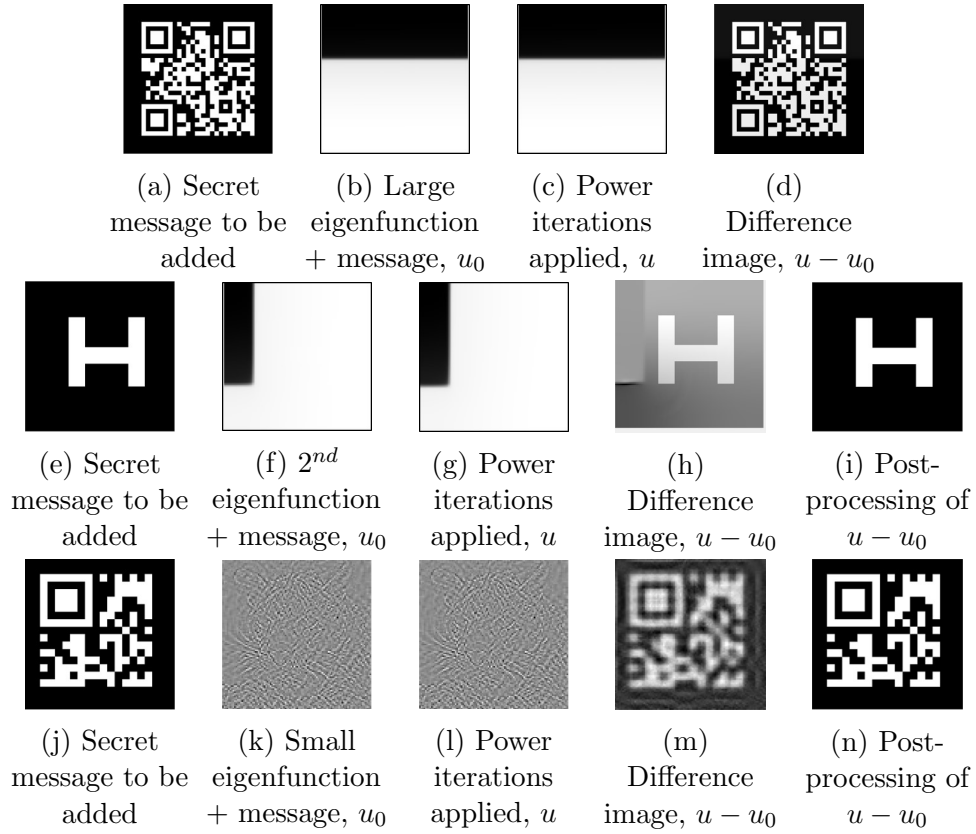


Figure 12: Examples of the encryption-decryption scheme for different messages and EPLL eigenfunctions. For each row, from left to right: a secret message; an eigenfunction with message added (u_0); after (500) power iterations applied (u); and their difference ($u - u_0$). Row 2: we use a "processed" eigenfunction (see Sec. 2.7) and perform simple segmentation as post-processing. Row 3 post-processing: locating the large square template of the message in the result, using a correlation matrix, then thresholding the central pixel of each image cell to determine its value.

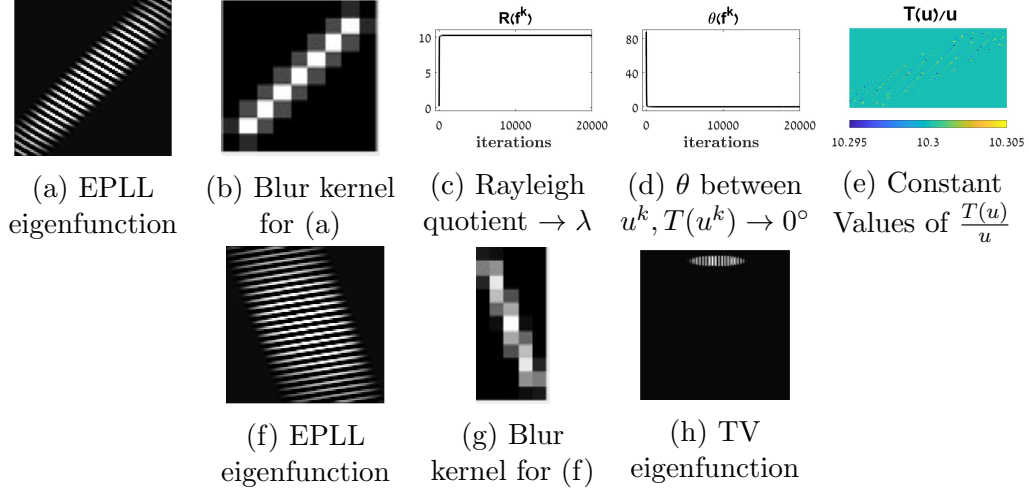


Figure 13: Eigenfunctions of deblurring operators. For the EPLL deblurring operator: eigenfunction (a) with eigenvalue $\lambda = 10.3001$ for motion kernel (b) (we validate this is an eigenfunction following Propositions 2-4), eigenfunction (f) with eigenvalue $\lambda = 10.3845$ for kernel (g). For the TV deblurring operator: eigenfunction (e) with $\lambda = 16.0913$.

blur kernels. Note that the straight but slightly rounded shapes of eigenfunctions correspond to the different kernel shapes, and are in accordance with the observations made in [30], regarding the behavior of the EPLL denoiser. We also show a large eigenfunction of the TV deblurring operator, generated using a Gaussian blur kernel. Note that the eigenfunction shape is in accordance with the convex nature of eigenfunctions of the TV denoiser [25]. For both operators, the eigenfunctions are textural objects - in accordance with the detail-enhancing nature of deblurring operators. Also, the resulting eigenvalues are larger than 1, as expected from detail-enhancing operators, and in accordance with Corollary 1.

4. Conclusions

We suggest a generalized numerical method for solving and analyzing nonlinear eigenproblems by adapting the well established power iteration. The method is suited for generic, non-linear operators, which may be "black-box" operators induced by image processing algorithms. We show theoretical results regarding the steady state properties of the process and show convergence for contraction operators (Lipschitz continuous). We also present analysis tools for validation. We demonstrate our method for two image denoising operators: the well-known functional-induced total-variation, and the "black-box" EPLL (which is based on image statistics of natural images). We show how to find eigenfunctions with large and small eigenvalues, and also several in an iterative process. The robustness of an eigenfunction to various degradations is demonstrated. Based on this insight we suggest an encryption-decryption application. Finally, we analyze eigenproblems for nonlinear non-convex image deblurring operators, apparently for the first time.

Acknowledgements. We acknowledge support by the Israel Science Foundation (grant No. 534/19) and the Technion Ollendorff Minerva Center.

References

References

- [1] R. Mises, H. Pollaczek-Geiringer, Praktische verfahren der gleichungsauflösung., J. of Applied Mathematics and Mechanics 9 (2) (1929) 152–164.
- [2] G. H. Golub, C. F. Van Loan, Matrix computations, Johns Hopkins U, Math. Sci., Johns Hopkins University Press, Baltimore, MD.

- [3] M. Hein, T. Bühler, An inverse power method for nonlinear eigenproblems with applications in 1-spectral clustering and sparse pca, in: *Advances in Neural Information Processing Systems*, 2010, pp. 847–855.
- [4] R. Z. Nossek, G. Gilboa, Flows generating nonlinear eigenfunctions, *J. of Scientific Computing* 75 (2) (2018) 859–888.
- [5] T. M. Feld, J.-F. Aujol, G. Gilboa, N. Papadakis, Rayleigh quotient minimization for absolutely one-homogeneous functionals., *Inv. Prob.*
- [6] J.-F. Aujol, G. Gilboa, N. Papadakis, Theoretical analysis of flows estimating eigenfunctions of one-homogeneous functionals, *SIAM J. on Imaging Sciences* 11 (2) (2018) 1416–1440.
- [7] X. Bresson, T. Laurent, D. Uminsky, J. H. von Brecht, An adaptive total variation algorithm for computing the balanced cut of a graph, *arXiv preprint arXiv:1302.2717*.
- [8] L. Bungert, M. Burger, Asymptotic profiles of nonlinear homogeneous evolution equations of gradient flow type, *arXiv preprint arXiv:1906.09856*.
- [9] A. I. Aviles-Rivero, N. Papadakis, R. Li, S. M. Alsaleh, R. T. Tan, C.-B. Schonlieb, Beyond supervised classification: Extreme minimal supervision with the graph 1-laplacian, *arXiv preprint arXiv:1906.08635*.
- [10] D. Zoran, Y. Weiss, From learning models of natural image patches to whole image restoration, in: *Int. Conf. on Computer Vision*, IEEE, 2011, pp. 479–486.
- [11] L. I. Rudin, S. Osher, E. Fatemi, Nonlinear total variation based noise removal algorithms, *Physica D: nonlinear phenomena* 60 (1-4) (1992) 259–268.
- [12] L. N. Trefethen, D. Bau III, *Numerical linear algebra*, Vol. 50, Siam, 1997.
- [13] E. Pohlhausen, Berechnung der eigenschwingungen statisch-bestimmter fachwerke, *ZAMM-J. of Applied Math. and Mech.* 1 (1) (1921) 28–42.
- [14] J. H. Wilkinson, *The algebraic eigenvalue problem*, Vol. 662, Oxford Clarendon, 1965.

- [15] W. E. Arnoldi, The principle of minimized iterations in the solution of the matrix eigenvalue problem, *Quarterly of applied mathematics* 9 (1) (1951) 17–29.
- [16] R. A. Horn, C. R. Johnson, *Matrix analysis*, Cambridge university press, 2012.
- [17] C. Daskalakis, C. Tzamos, M. Zampetakis, A converse to banach’s fixed point theorem and its cls-completeness, in: *Proc. of the 50th Annual ACM SIGACT Symp. on Theory of Computing*, ACM, 2018, pp. 44–50.
- [18] S.-J. Wu, M. T. Chu, Markov chains with memory, tensor formulation, and the dynamics of power iteration, *Appl. Mathematics and Computation* 303 (2017) 226–239.
- [19] M. T. Chu, S.-j. Wu, On the second dominant eigenvalue affecting the power method for transition probability tensors.
- [20] T. G. Kolda, J. R. Mayo, Shifted power method for computing tensor eigenpairs, *SIAM J. on Matrix Analysis and Applications* 32 (4) (2011) 1095–1124.
- [21] F. E. Browder, W. Petryshyn, The solution by iteration of nonlinear functional equations in banach spaces, *Bulletin of the Am. Mathematical Soc.* 72 (3) (1966) 571–575.
- [22] M. Benning, M. Burger, Ground states and singular vectors of convex variational regularization methods, *Methods and Applications of Analysis* 20 (4) (2013) 295–334.
- [23] M. Burger, G. Gilboa, M. Moeller, L. Eckardt, D. Cremers, Spectral decompositions using one-homogeneous functionals, *SIAM Journal on Imaging Sciences* 9 (3) (2016) 1374–1408.
- [24] L. Bungert, M. Burger, A. Chambolle, M. Novaga, Nonlinear spectral decompositions by gradient flows of one-homogeneous functionals, *arXiv preprint arXiv:1901.06979*.
- [25] G. Gilboa, Beyond convex analysis - decompositions with nonlinear flows, in: *Nonlinear Eigenproblems in Image Processing and Computer Vision*, Springer, 2018, pp. 133–140.

- [26] A. Chambolle, An algorithm for total variation minimization and applications, *Journal of Mathematical imaging and vision* 20 (1-2) (2004) 89–97.
- [27] O. Katzir, On the scale-space of filters and their applications, Master’s thesis, Technion, Israel Institute of Technology, Haifa, Israel (2017).
- [28] Y. Meyer, Oscillating patterns in image processing and nonlinear evolution equations: the fifteenth Dean Jacqueline B. Lewis memorial lectures, Vol. 22, American Mathematical Soc., 2001.
- [29] L. Bungert, M. Burger, Solution paths of variational regularization methods for inverse problems, *Inverse Problems*.
- [30] T. R. Shaham, T. Michaeli, Visualizing image priors, in: *European Conf. on Computer Vision*, Springer, 2016, pp. 136–153.
- [31] M. F. Schmidt, M. Benning, C.-B. Schönlieb, Inverse scale space decomposition, *Inverse Problems* 34 (4) (2018) 045008.